

HYBRID FINITE-DISCRETE ELEMENT MODELLING OF BLAST-INDUCED EXCAVATION DAMAGED ZONE IN THE TOP-HEADING OF DEEP TUNNELS

Huaming An^{1}, Hongyuan Liu², Xuguang Wang³, Jianjun Shi¹, Haoyu Han²*

- 1. School of Civil & Resource Engineering, University of Science & Technology Beijing, China. Email Huaming.an@yahoo.com*
- 2. School of Engineering and ICT, University of Tasmania, Australia.*
- 3. Beijing General Research Institute of Mining & Metallurgy, China.*

ABSTRACT

A hybrid finite-discrete element method (FEM/DEM) is introduced to model the excavation damage zone induced by blast in a deep tunnel. The key components of the hybrid finite-discrete element method, i.e. transition from continuum to discontinuum through fracture and fragmentation, and detonation-induced gas expansion and flow through fracturing rock, are introduced in detail. The stress and crack initiation and propagation of an uniaxial compression test is then modelled by the proposed method and compared with those well documented in literature to calibrate the hybrid FEM/DEM. The modelled stress-loading displacement curve presents a typical failure process of brittle materials. The calibrated method is then used to model the stress and crack initiation and propagation induced by blast for the last step of excavation in a deep tunnel. A separation contour, which connects the borehole through the radial cracks from each borehole, is observed during the excavation process. The newly formed tunnel wall is produced and the main components of excavation damage zone (EDZ) are obtained. Therefore, the proposed treatment has the capabilities of modelling blast-induced EDZ and rock failure process. It is concluded that the hybrid FEM/DEM is a valuable numerical tool for studying excavation damage zone in terms of crack initiation and propagation and stress distribution.

KEYWORDS

Hybrid FEM/DEM, Excavation Damage Zone (EDZ), Rock Blast, Deep Tunnel

INTRODUCTION

As one of the most efficient ways for breaking rock, blasting is widely employed in underground excavation such as tunnelling, mining and shafting. However, blasting inevitably causes disturbance to the original state of rock in the form of creation of new fracture, closure and opening of pre-existing fractures, and redistribution of stresses [1]. The disturbance zone with properties and conditions irreversibly changed is often referred to as Excavation Damaged Zone (EDZ) or the Damaged Rock Zone (DRZ) [2, 3]. Significant efforts have been spent worldwide in gaining an understanding of EDZ over the last few decades, especially characterizing and classifying EDZ [3], which includes the studies on EDZ around hydraulic tunnels in Russia [4] and that around in the Three Gorges Dam in China [5, 6], and several international workshops on EDZ [2, 7].

Nowadays, the fast development of the computer technology makes it become possible to complete large-scale numerical calculations in a short time. Correspondingly, various numerical methods have been implemented to simulate the rock blasting process including EDZ induced by rock blasting. According to the reviews conducted by Preece et al. [8], Latham et al. [9], Saharan et al. [10] and Perras et al. [11], continuous methods, e.g. finite element method, and discontinuous methods, e.g. discrete element method, have been mainly implemented to investigate the rock blasting processes. The continuous method usually focuses on modelling the blast-induced damage before rock fragmentation while the discontinuous method concentrates more on the detonation-induced crack propagation and resultant fragment movement during and after rock fragmentation. Therefore, it may be a better choice to combine the continuous and discontinuous methods to investigate the blasting-induced EDZ. Correspondingly, this paper is attempting to model the EDZ induced by rock blasting in a deep tunnel using a combined continuous-discontinuous method, i.e. the hybrid finite-discrete element method (FEM/DEM).

Hybrid FEM/DEM

In the hybrid finite-discrete element method (FEM/DEM), a hybrid FEM/DEM model can include a single discrete body or a number of interactive discrete bodies, each of which is of general shape and size and is modelled by a single discrete element. Each individual element is then discretized into the finite elements to analyze the deformability, fracture, and fragmentation. The essential components of the hybrid FEM/DEM consist of contact detection and interaction among those individual discrete bodies, deformability and transition from continuum to discontinuum through fracture and fragmentation of individual discrete bodies, temporal integration scheme and computational fluid dynamics [12].

A hybrid FEM/DEM comprising these key components has been implemented by Liu et al. [12] on the basis of their previous enriched finite element codes RFPA-RT2D [13] and TunGeo3D [14], and the open-source combined finite-discrete element libraries Y2D and Y3D originally developed by Munjiza [15] and Xiang et al. [16], respectively, which is to be used in this study.

The modelling of blast-induced EDZ in deep tunnel involves the fracture and fragmentation of rocks, and expansion of high pressured gas. Correspondingly, the transition from continuum to discontinuum and the gas expansion are the key components for the blast-induced EDZ modelling by hybrid FEM/DEM, which, therefore, are introduced briefly here while detailed introduction can be found in a recent paper published by the authors [17].

Transition from continuum to discontinuum

In the hybrid FEM/DEM, the discrete elements are discretized into the finite elements and those finite elements are bonded together through a four-node joint element. The enforcing constraint of the finite elements involves a bonding stress, which is taken to be a function of the separation between the surfaces of joints elements. The cracks are assumed to coincide at the surfaces of the joint elements during fracturing. The separation δ at any point can be divided into two components in Equation 1

$$\delta = \delta_n n + \delta_s t \quad (1)$$

where n and t are the unit vectors in the normal and tangential directions, respectively, of the surface at such a point, δ_n and δ_s are the magnitudes of the components of δ on the normal and tangential directions, respectively. Figure 1 shows the relationship between the bonding stress and

opening/sliding displacement under tension and shear conditions. If the opening of the joints elements, i.e. the separations in the normal direction δ_n or in the tangential direction δ_s , reach critical displacements i.e. δ_{np} in normal direction or δ_{sp} in tangential direction, determined by the tensile strength σ_t or the shear strength σ_c of the element, damages are assumed to occur. As the separations of the joint element increase, $\delta_n > \delta_{np}$ in normal direction or $\delta_s > \delta_{sp}$ in tangential direction, the bonding stresses gradually decrease. In terms of the opening in normal direction, when the opening of the joint element is beyond the ultimate opening displacement δ_{nu} , the joint element is broken and the tensile failure occurs. With regard to separation of the joint elements in tangential direction, while the opening of the joint element exceeds a residual opening displacement δ_{sr} , the shear failure occurs and the bonding stress becomes a purely frictional resistance. The relationships between the bonding stress and the opening of the joint element can be described in Equations 2 and 3 for the tension and shear situations, respectively.

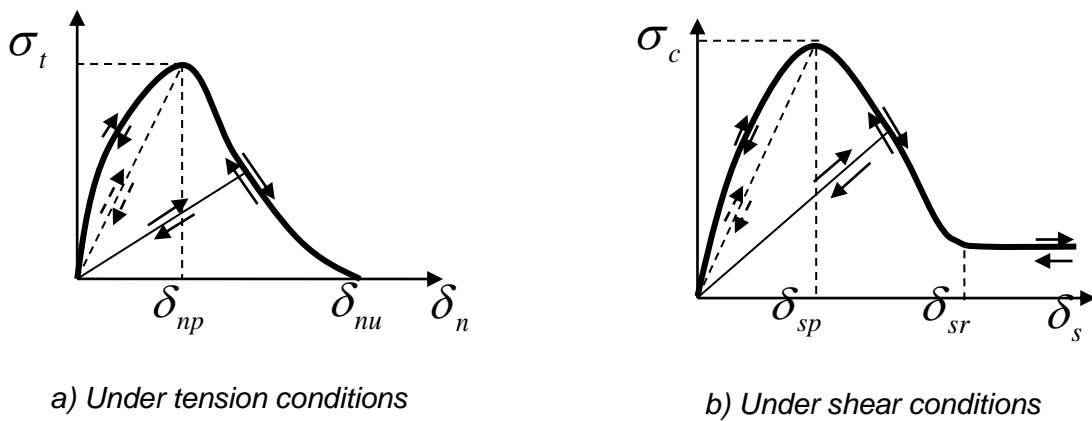


Fig. 1 - Relationship between the bonding stress and opening/sliding displacement under tension and shear conditions

$$\sigma_n = \begin{cases} f(D) \sigma_t, & \text{if } 0 \leq \delta \leq \delta_{nu} \\ 0, & \text{if } \delta \geq \delta_{nu} \end{cases} \quad (2)$$

$$\tau = \begin{cases} \left[2 \frac{\delta_s}{\delta_{sp}} - \left(\frac{\delta_s}{\delta_{sp}} \right)^2 \right] \sigma_c, & \text{if } 0 \leq \delta_s \leq \delta_{sp} \\ g(D) \sigma_c, & \text{if } \delta_{sp} \leq \delta_s \leq \delta_{sr} \\ \sigma_n \tan(\theta_f), & \text{if } \delta_s \geq \delta_{sr} \end{cases} \quad (3)$$

where D is the damage variable between 0 and 1, $f(D)$ and $g(D)$ are damage functions described in the mechanical damage model [13], and θ_f is the joint residual friction angle.

Detonation-induced gas expansion and flow through fracturing rock

The modelling of detonation-induced EDZ involves in the interaction of the high pressured detonation products with surrounding rock mass and the gas flow through fracturing rock mass. In the hybrid FEM/DEM, the first section, i.e. the interaction between detonation products and surrounding rocks, is modelled through a pressure-time histories curve generated from commercial finite element codes AUTODYN through the Jones-Wilkens-Lee (JWL) equation of state (EOS) in Equation 4.

$$P = A \left(1 - \frac{\omega \rho}{R_1 \rho_0} \right) \exp \left(-R_1 \frac{\rho_0}{\rho} \right) + B \left(1 - \frac{\omega \rho}{R_2 \rho_0} \right) \exp \left(-R_2 \frac{\rho_0}{\rho} \right) + \frac{\omega \rho^2}{\rho_0} E_{m0} \quad (4)$$

where P is the instantaneous pressure at any time, A , B , R_1 , R_2 and ω are the material constants, ρ_0 and ρ are the densities of the explosive and the detonation products, respectively, and E_{m0} is the specific energy. The second section, i.e. the gas flow through fracturing rock mass, is modelled through a simple model consisting of a gas zone and constant area ducts. The gas zone is defined as a circle around the borehole and the explosive gas is presented only inside the circle. The cracks around the borehole are assumed to be the constant area ducts in the gas zone. The spatial and temporal distribution of the gas pressure in the gas zone are determined by an iteration procedure. Thus the process of gas exerting pressure on the crack walls and expanding the cracks can be modelled. More details can be found in the literatures by Munjiza et al. [15, 18].

CALIBRATION OF THE PROPOSED HYBRID FINITE-DISCRETE ELEMENT METHOD

To calibrate the hybrid finite-discrete element method, the rock fracture processes in a quasi-static uniaxial compression test is modelled and the obtained results are compared with those well documented in literatures.

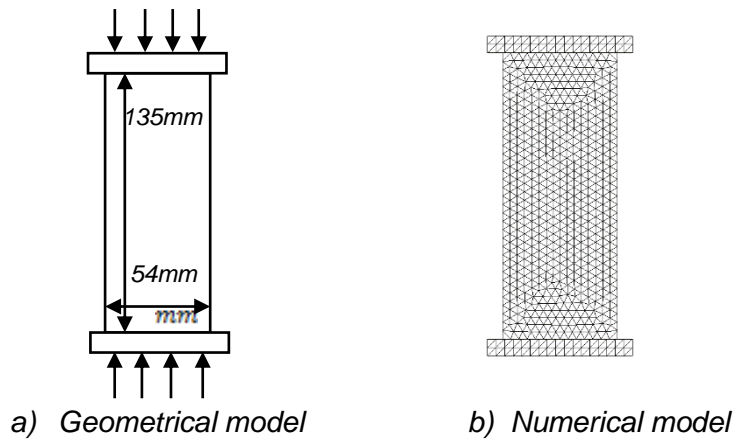


Fig. 2 - Geometrical and numerical model for uniaxial compression test

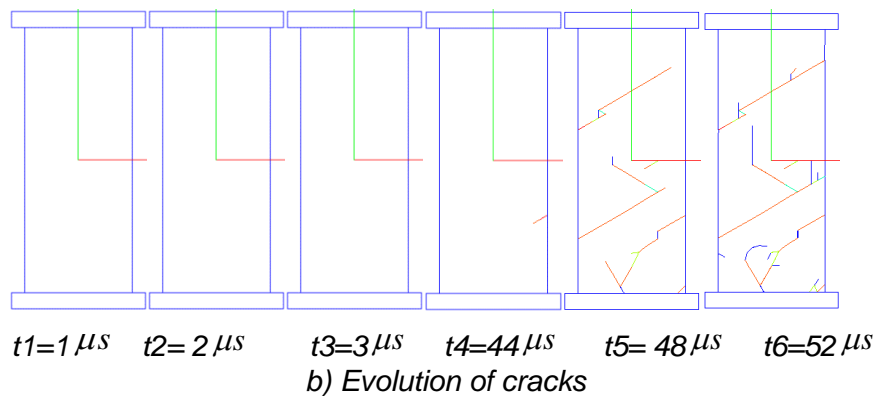
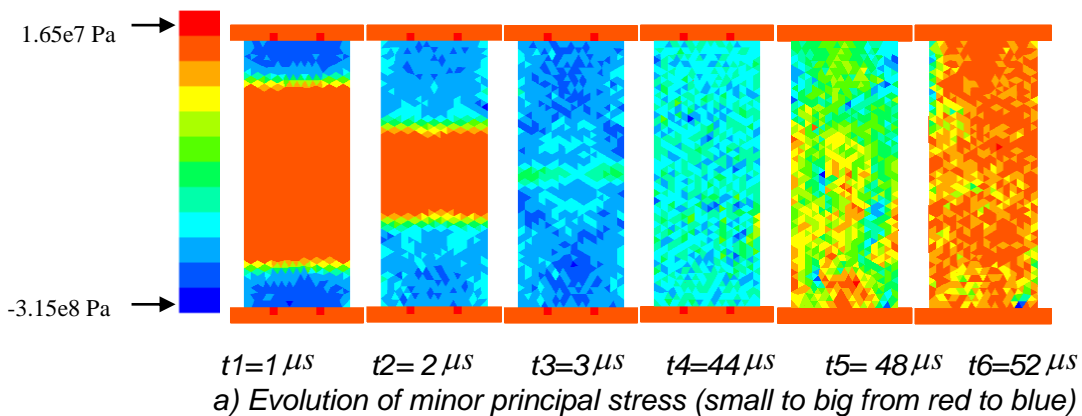


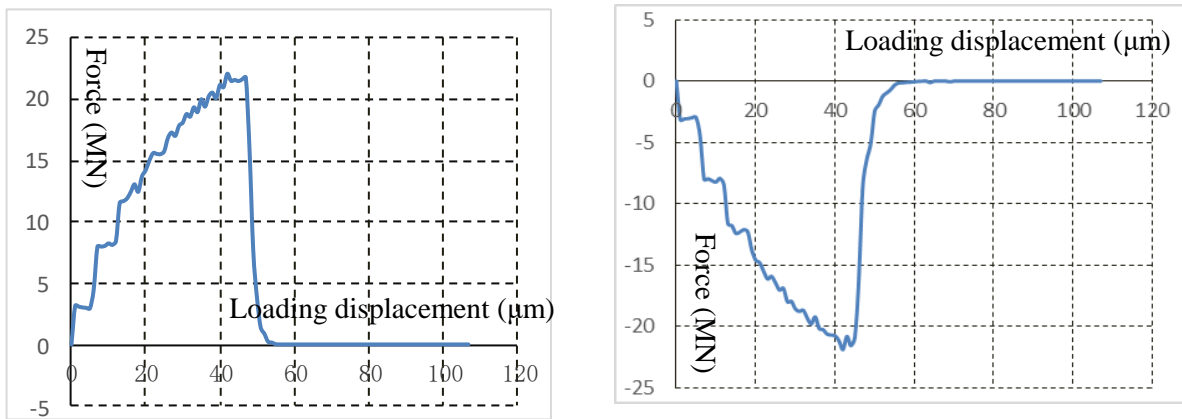
Fig.3 - Modelled failure process during the uniaxial compression test

The uniaxial compression test is simplified as a plane stress problem and a vertical section is considered as shown in Figure 2. The material properties of the rock specimen are Young's modulus $E = 60 \text{ GPa}$, Poisson's ratio $\nu = 0.26$, density $\rho = 2600 \text{ Kg m}^{-3}$, tensile strength $\sigma_t = 20 \text{ MPa}$, compressive strength $\sigma_c = 200 \text{ MPa}$, internal friction angle $\Phi = 30^\circ$, surface friction coefficient $u = 0.1$, mode I fracture energy $G_{fl} = 50 \text{ N m}^{-1}$, mode II fracture energy $G_{fll} = 250 \text{ N m}^{-1}$.

The material properties of the loading plates follow those of standard steels.

A constant velocity of 1 m s^{-1} is applied on both, the top and bottom plates so that they move towards each other to load the specimen located in between them. It may be worthy pointing out that the applied loading rates are much higher than those used in laboratory static experiments. Nevertheless, the applied loading rates should not influence the rock properties significantly as these are still much smaller than the certain threshold level according to laboratory dynamic experiments [19]. The reasons of applying relatively bigger loading rates are that the calculation time can be significantly reduced.

As shown in Figure 3a) and b), the modelled progressive failure process during the uniaxial compression test is illustrated in terms of the distributions of minor principal stress and cracks respectively. The value of the minor principal stress is indicated by the colour legend in the left side of Fig.3. Moreover, the red colour represents shear failure while the blue represents tensile failure and model boundaries in Figure 3b. As loads are applied on the two plates, the stresses transfer to the specimen and concentrate on the top and bottom of the specimen. Then the stresses (from top and bottom) propagate to the center of the specimen and meet at $3 \mu\text{s}$. No crack occurs until $44 \mu\text{s}$ (Figure 3b) and the force-loadings are increasing (Figure 4). A crack firstly occurs at $44 \mu\text{s}$ (Figure 3b) when the force-loadings reach their peaks (Figure 4a and b). After that, the force-loadings drop dramatically from their peaks to the bottoms (Figure 4a and b from $48 \mu\text{s}$ to $55 \mu\text{s}$) which indicates the specimen loses its ability of carrying loads. Meanwhile, two almost parallel shear cracks form at $52 \mu\text{s}$ (Figure 3b).



a) Top force-loading displacement curve

b) Bottom force-loading displacement curve

Fig. 4 - Force-loading displacement curve during the uniaxial

Obviously, the modelled results reproduce the brittle rock failure process under loading and agree with laboratory results [20]: a nearly linear loading increase region (Figure 4 from 0 to $44 \mu\text{s}$), a big jump from the peak value to bottom (Figure 4 from 44 to $55 \mu\text{s}$) and a post failure region (Figure 4 from 55 to $100 \mu\text{s}$).

MODELLING OF EXCAVATION DAMAGED ZONE IN DEEP TUNNEL BY BLAST

In this section, a perimeter blasting techniques, i.e. smooth blasting, are adopted for the excavation of a deep tunnel. Figure 5 illustrates the geometry and numerical model of the top heading in exaction tunnel. A $22m \times 22m$ square is taken as the boundary. The tunnel is assumed to be located 450m underground. The in-situ stresses around the tunnel are major principal stress $\sigma_1 = 30MPa$, which lies in the horizontal direction, and minor principal stress $\sigma_3 = 10MPa$, which lies in the vertical direction. In order to save the computational time, only the last steps of top heading excavation are modelled here.

As shown in Figure 5a, 46 boreholes with diameters of 0.1m are set around the top heading. The space between boreholes is 0.4m and the blasting burden is 0.5m. As shown in Figure 5b, triangular elements are employed to discretize the model, and dense elements are employed in the interested area. Due to symmetry, only a half of the model is simulated, in which the symmetrical and bottom boundaries are fixed in x and y directions, respectively, while other boundaries are set as in-situ stress, e.g. $\sigma_1 = 30MPa$ in x direction and $\sigma_3 = 10MPa$ in y direction. The parameters of the rock mass underground follow those in the uniaxial compression test.

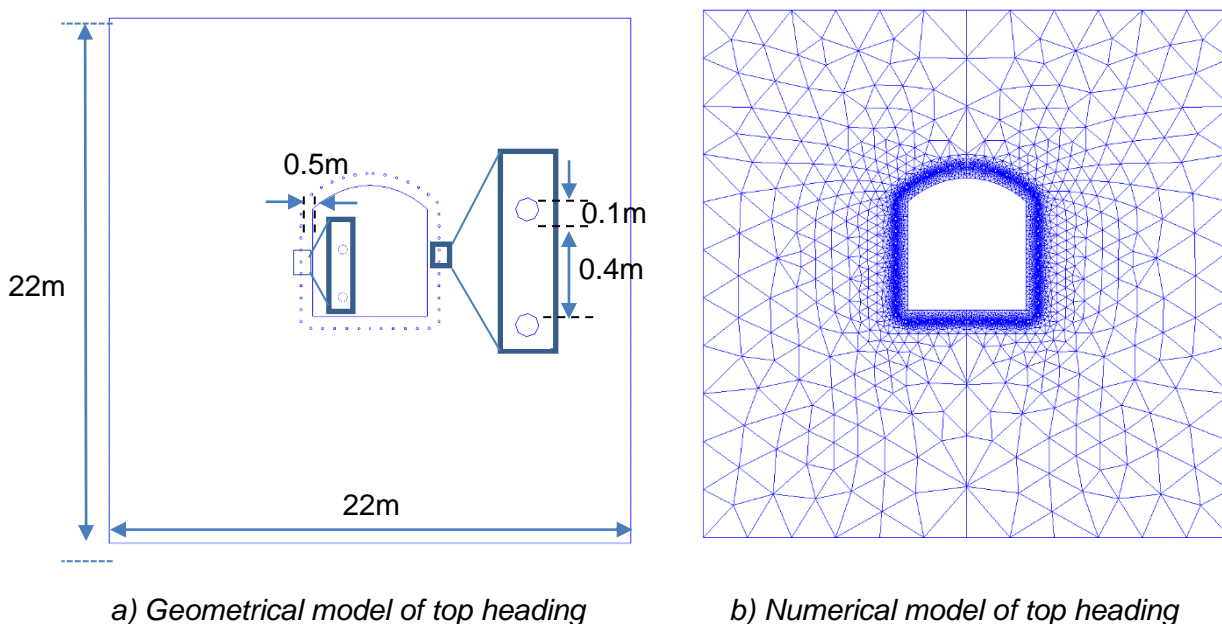


Fig. 5 - Geometrical model and numerical model for top heading

Stress and crack initiation and propagation

Figure 6 visually illustrates the evolution of the minor principal stress in the top heading of the tunnel while the corresponding fracture initiation and propagation process is depicted in Figure 7. It should be noted that following the sign convention in solid mechanics, the compressive stress is taken as negative while the tensile stress is regarded as positive. Moreover, the colour in the Figure 6 represents the size of the minor principal stress (compressive stress) and the magnitudes can be referred to the legend shown in Figure 6a). Moreover, the red colour represents tensile failures while the boundaries and shear failures are marked as blue colour in Figure 7.

As can be seen in Figure 6, the in-situ stresses are applied on the left, right and top boundaries of the model, which hence initiate from the three boundaries and propagate towards the tunnel wall. The in-situ stresses arrive at the tunnel wall at 0.40ms (Figure 6b). The stresses are reflected from the tunnel wall and interact with the stress from the boundaries. Eventually, the in-situ stress equilibrium achieves (Figure 6c). A few cracks are observed (Figure 7b) around the tunnel wall due to the in-situ stress intensive. As the explosives in the 46 boreholes are detonated simultaneously at 1.45 ms, the contained chemical charge in the boreholes react rapidly [21]. As a result, high-pressure gases from each borehole are created and interact with the rock mass surrounding the boreholes and immediately intense stress waves initiate and propagate rapidly out of the borehole as illustrated in Figure 6d). It is worth noting that due to the relatively lower initial gas pressure adopted for the smooth blasting, crush zones, in which the rock mass is supposed to be crushed and scattered immediately around a borehole, are not clearly formed. Instead, cracked zones are produced directly (Figure 7c). The blast induced stresses continue to propagate outwards and a strong stress zone along the tunnel wall are formed (Figure 6d, e and f). While stress waves continue to propagate outwards, the cracks around the boreholes propagate radically and interact with cracks from the adjacent boreholes to form a crack contour (Figure 7d). As a result, the boreholes are connected together by the cracks to form a single chamber. Thus, the cracks mainly propagate along crack contour due to the high pressure gas in the chamber. Additionally, more cracks initiate at the tunnel boundary because of the stresses reflection and eventually the excavated rock mass is broken into fragments as illustrated in Figures 7f, g and h). Moreover, long cracks continue to propagate by the expansion of the high pressure gas (Figures 7 e-h). Finally, the excavated rock mass is pushed out by the high pressure gas and a new tunnel wall is formed (Figure 6i, Figure 7h). Figure 7i illustrates the newly formed tunnel wall after removing the fragments and the EDZ around the tunnel wall.

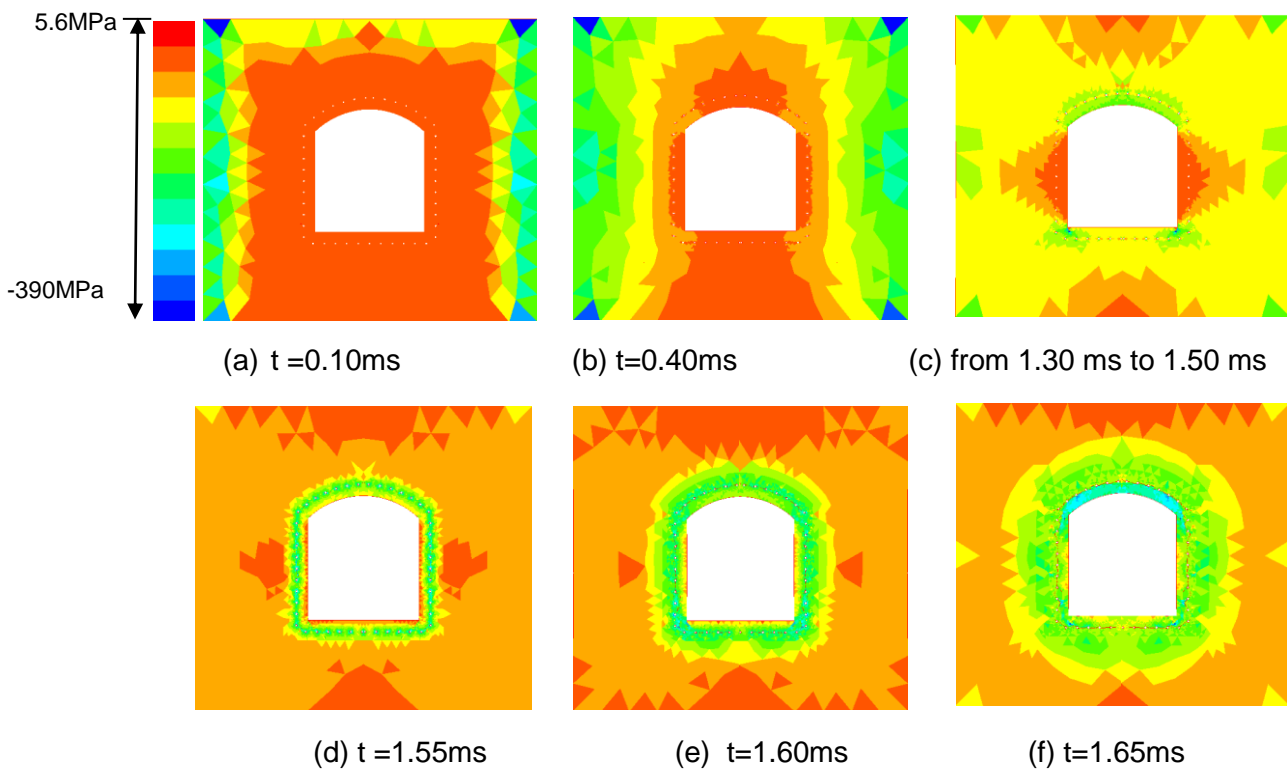


Fig. 6 - Minor principal stress propagation for smooth blasting in the top heading of a deep tunnel

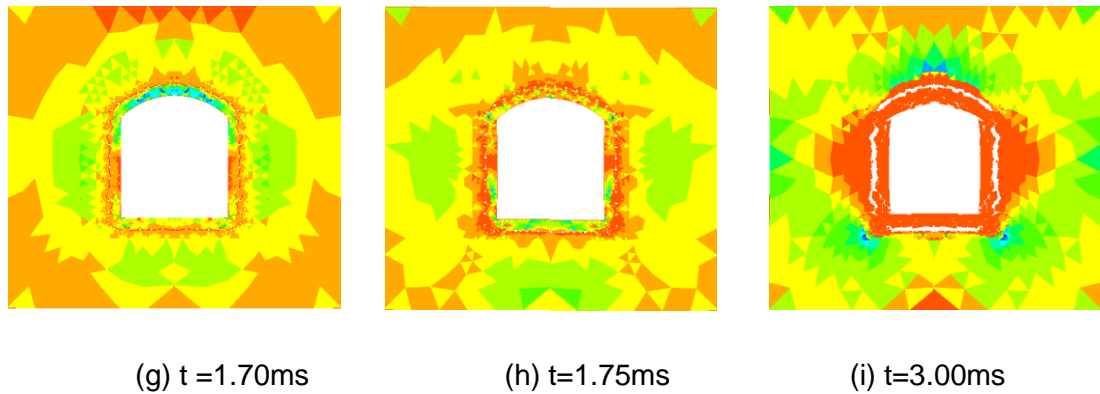


Fig. 6 - Minor principal stress propagation for smooth blasting in the top heading of a deep tunnel

Thus, it can be seen from Figures 6 and 7 that the hybrid finite-discrete element method successfully modelled the last step of the top heading excavation by blast in a deep tunnel. A newly formed wall is produced and the EDZ around the tunnel wall is induced (Figure 7i). The EDZ can be divided into inner damage zone (Figure 7i-A between tunnel wall and the red dash line), outer damage zones (Figure 7i-B) where the rock properties are sharply changed, and disturbed zone (Figures 7i-C) where stress is redistributed. Therefore, the simulated result agrees well with the literatures [1, 22].

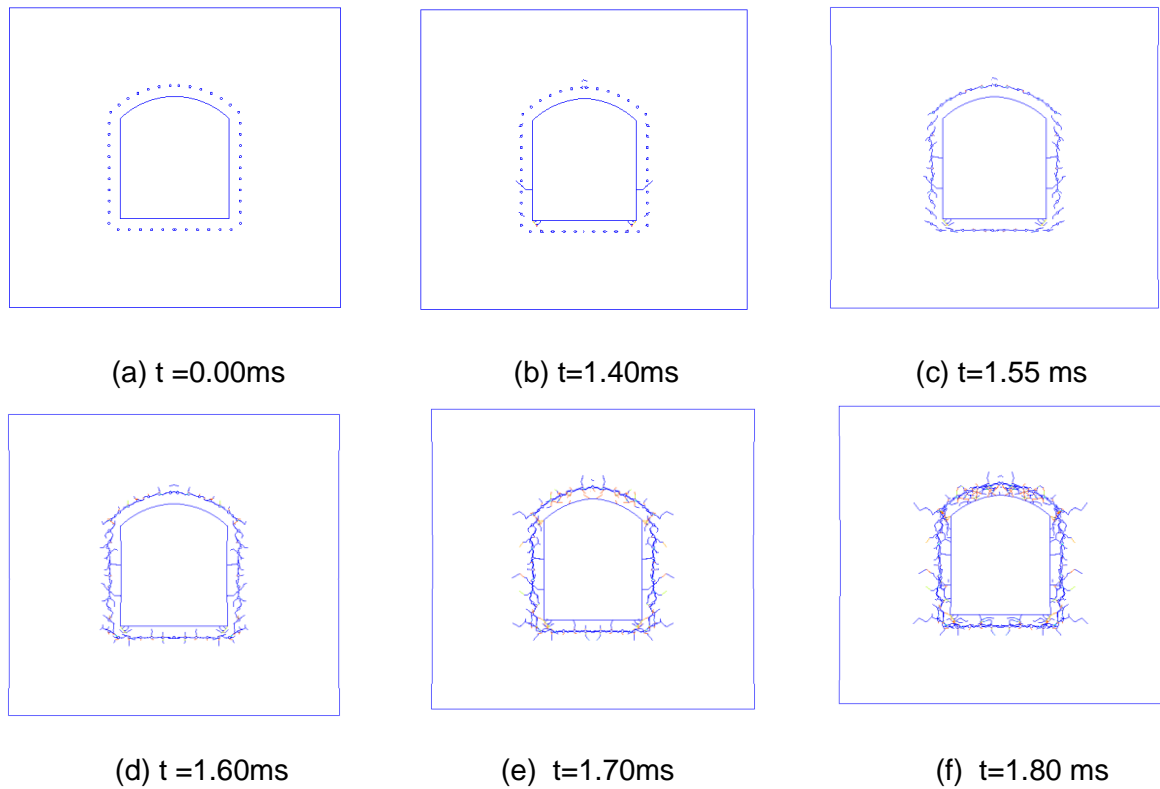


Fig. 7 - Fracture initiation and propagation induced by smooth blasting in top heading of a deep tunnel

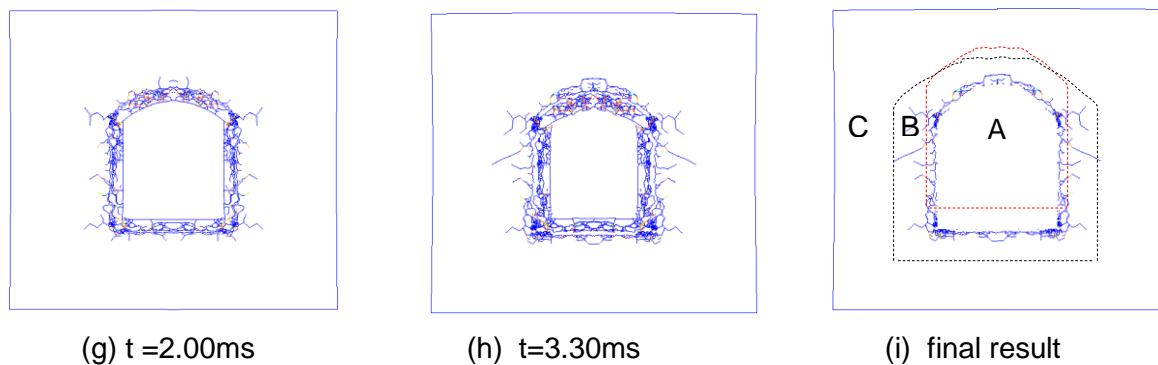


Fig. 7 - Fracture initiation and propagation induced by smooth blasting in top heading of a deep tunnel

CONCLUSION

In this paper, a hybrid FEM/DEM is proposed to model the blast induced EDZ in a deep tunnel. Among the key components of the hybrid finite-discrete element method, transition from continuum to discontinuum through fracture and fragmentation makes the proposed method distinguish from the continuum-based method, e.g. FEM, and discontinuum-based method, e.g. DEM. The numerical model of the hybrid method comprises of one or a number of discrete elements which are discretized into finite elements. The transition from continuum to discontinuum through fracture and fragmentation is implemented through separating the adjacent finite elements, which are bonded together by four-node joint elements. Additionally, detonation-induced gas expansion and flow through fracturing rock play significant roles in rock blasting. Hereby a pressure-time histories curve generated from commercial finite element codes AUTODYN through the Jones-Wilkens-Lee (JWL) equation of state (EOS) is implemented in the hybrid method to model the gas expansion process, while a simple model consisting of a gas zone and constant area ducts is adopted to model the gas flow through fracturing rock mass.

The proposed method is then used to model the rock failure process in uniaxial compression test to calibrate the hybrid FEM/DEM by comparing the modelled failure process and force-loading displacement curve with those in literatures. The calibrated method is then used to model the EDZ in a deep tunnel to demonstrate the potential application of the hybrid method. The stress and crack initiation and propagation are modelled and the EDZ is obtained. It is found that the modelled results of EDZ show a good agreement with those found in literature. Therefore, it is concluded that the hybrid FEM/DEM has the capabilities of modelling the rock failure processes by blast. Moreover, the hybrid finite discrete element method is a valuable numerical tool for the study of EDZ in tunnels.

ACKNOWLEDGEMENTS

The first author completed this research at the University of Tasmania under the supervision of the second author, which is partly supported by a two-year joint PhD scholarship provided by China Scholarship Council (CSC). The CSC's support is greatly appreciated

REFERENCES

- [1] Sato, T., T. Kikuchi, and K. Sugihara, 2000. In-situ experiments on an excavation disturbed zone induced by mechanical excavation in Neogene sedimentary rock at Tono mine, central Japan. *Engineering geology*, Vol. 56(1): 97-108.
- [2] Martino, J., 2003. The 2002 international EDZ workshop: the excavation damaged zone—cause and effects. Atomic Energy of Canada Limited.
- [3] Saiang, D., 2008. Behaviour of blast-induced damaged zone around underground excavations in hard rock mass, Doctoral Thesis, Luleå university of technology, Luleå, Sweden.
- [4] Mostkov, V., 1979. USSR experience in construction of hydraulic tunnels. Electric Power Research Institute (Report) EPRI EL, 81-88.
- [5] Deng, J., C. Lee, and X. Ge, 2001. Characterization of the disturbed zone in a large rock excavation for the Three Gorges Project. *Canadian geotechnical journal*, Vol. 38(1): 95-106.
- [6] Sheng, Q., et al., 2002. Estimating the excavation disturbed zone in the permanent shiplock slopes of the Three Gorges Project, China. *International Journal of Rock Mechanics and Mining Sciences*, Vol. 39(2): 165-184.
- [7] Tsang, C.-F., F. Bernier, and C. Davies, 2005. Geohydromechanical processes in the Excavation Damaged Zone in crystalline rock, rock salt, and indurated and plastic clays—in the context of radioactive waste disposal. *International Journal of Rock Mechanics and Mining Sciences*, Vol. 42(1): 109-125.
- [8] Preece, D., et al., 1994. Computer Simulation of Rock Blasting: A Summary of Work from 1987 through 1993. SAND94-1027, Sandia National Laboratories.
- [9] Latham, J.P., A. Munjiza, and P. Lu, 1999. Rock fragmentation by blasting—a literature study of research in the 1980's and 1990's. *Fragblast*, Vol. 3(3): 193-212.
- [10] Saharan, M., H. Mitri, and J. Jethwa, 2006. Rock fracturing by explosive energy: review of state-of-the-art. *Fragblast*, Vol.10(1-2): 61-81.
- [11] Perras, M.A., M.S. Diederichs, and T. Lam, 2010. A review of excavation damage zone in sedimentary rocks with emphasis on numerical modelling for EDZ definition. in *Proceedings of the 2010 Canadian Geotechnical Conference*, Calgary.
- [12] Liu, H., Y. Kang, and P. Lin, 2013. Hybrid finite-discrete element modeling of geomaterials fracture and fragment muck-piling. *International Journal of Geotechnical Engineering*, Vol. 9(2), 115-131.
- [13] Liu, H., et al., 2004. Numerical studies on the failure process and associated microseismicity in rock under triaxial compression. *Tectonophysics*, Vol. 384(1):149-174.
- [14] Liu, H., 2010. A numerical model for failure and collapse analysis of geostuctures. *Australian Geomechanics*, Vol. 45(3): 11-19.
- [15] Munjiza, A., *The Combined Finite-Discrete Element Method*. 2004: Wiley Online Library.
- [16] Xiang, J., A. Munjiza, and J.P. Latham., 2009. Finite strain, finite rotation quadratic tetrahedral element for the combined finite–discrete element method. *International journal for numerical methods in engineering*, Vol. 79(8): 946-978.

- [17] An, H., et al., 2017. Hybrid finite-discrete element modelling of dynamic fracture and resultant fragment casting and muck-piling by rock blast. *Computers and Geotechnics*, 81:322-345.
- [18] Munjiza, A., J. Latham, and K. Andrews, 2000. Detonation gas model for combined finite- discrete element simulation of fracture and fragmentation. *International Journal for Numerical Methods in Engineering*, Vol. 49(12): 1495-1520.
- [19] Zhang, Z., 2001. Laboratory studies of dynamic rock fracture and in-situ measurements of cutter forces for a boring machine, Doctoral Thesis, Lulea university of technology, Lulea, Sweden
- [20] Wawersik, W. and C. Fairhurst, 1970. A study of brittle rock fracture in laboratory compression experiments. *International Journal of Rock Mechanics and Mining Sciences & Geomechanics Abstracts*, Vol.7(5), 561 IN7, 565-564 IN 14-575.
- [21] Kutter, H. and C. Fairhurst, 1971. On the fracture process in blasting. in *International Journal of Rock Mechanics and Mining Sciences & Geomechanics Abstracts*, Vol.181-202.
- [22] Kuzyk, G.W. and J.B. Martino, 2008. Development of excavation technologies at the Canadian Underground Research Laboratory. *International Conference Underground Disposal Unit Design & Emplacement Processes for a Deep Geological Repository*, Prague. Czech Republic.